Research Square

Preprints are preliminary reports that have not undergone peer review.
They should not be considered conclusive, used to inform clinical practice,
or referenced by the media as validated information.

Recurrence entropy-based characterization of spatial patterns

Bruno Rafael Reichert Boaretto

bruno.boaretto@unifesp.br

Universidade Federal de São Paulo

Matheus Di Domenico

Universidade Federal do Paraná

Thiago de Lima Prado

Universidade Federal do Paraná

Sergio Roberto Lopes

Universidade Federal do Paraná

Elbert Einstein Nehrer Macau

Universidade Federal de São Paulo

Cristina Masoller

Universitat Politècnica de Catalunya

Article

Keywords: recurrence entropy, spatial patterns, recurrence microstates, texture analysis, pattern characterization

Posted Date: November 3rd, 2026

DOI: https://doi.org/10.21203/rs.3.rs-11295573/v1

License: This work is licensed under a Creative Commons Attribution 4.0 International License.
Read Full License

Additional Declarations: No competing interests reported.

Recurrence entropy-based characterization of spatial patterns

Bruno R. R. Boaretto[1,2*], M. Di Domenico[3], T. L. Prado[3], S. R. Lopes[3], Elbert E. N. Macau[1], Cristina Masoller[2]

[1]Institute of Science and Technology, Universidade Federal de São Paulo, 12247-014, São José dos Campos, São Paulo, Brazil.
[2]Department of Physics, Universitat Politecnica de Catalunya, 08222, Terrassa, Barcelona, Spain.
[3]Departamento de Física, Universidade Federal do Paraná, 81531-980, Curitiba, Paraná, Brazil.

*Corresponding author(s). E-mail(s): bruno.boaretto@unifesp.br;

Abstract

The identification and characterization of spatial patterns play an important role in fields ranging from medical imaging and materials science to laser physics and complex systems. Here, we introduce a recurrence-based framework for the analysis of two-dimensional patterns by extending concepts originally developed for nonlinear time series analysis. Spatial recurrence data are generated from pixel arrays and decomposed into recurrence motifs, whose statistical distribution is used to construct entropy-based descriptors of spatial organization. By systematically varying the recurrence threshold, we obtain a two-dimensional representation defined by the threshold and its associated recurrence entropy, providing a compact and interpretable feature space for pattern characterization. The proposed framework is validated using synthetic datasets, including fractional Brownian surfaces and Turing patterns, as well as real-world textures from the Kylberg dataset. The results show that recurrence entropy provides a complementary description of spatial organization, capturing structural changes associated with variations in spatial correlations and texture organization.

Keywords: recurrence entropy; spatial patterns; recurrence microstates; texture analysis; pattern characterization

1 Introduction

Spatial patterns emerge in a broad range of physical, biological, and technological systems, and their quantitative characterization is relevant to applications in diverse areas, including medical imaging, biotechnology, nanomaterials and materials science, computer vision, urban morphology and landscape characterization, remote sensing and Earth observation sciences [1–20]. In nonlinear physics and complex systems, spatial descriptors based on information-theory measures have been used to characterize textures, art works, laser speckle patterns and investigate transitions in vegetation fields and climatological spatio-temporal data [21–28]. These diverse applications motivate the development of descriptors capable of capturing relevant aspects of spatial organization in a general and interpretable manner.

Here, we introduce a recurrence-based framework for characterizing spatial patterns through the entropy of local recurrence configurations. For each pixel, recurrence is evaluated with its eight neighboring pixels, i.e., the pixels immediately surrounding it, according to a prescribed threshold, generating a binary configuration that defines a recurrence motif. The distribution of these motifs across the image describes how local recurrence configurations are organized and provides the basis for computing recurrence entropy [29, 30]: repetitive spatial structures tend to favor a smaller set of motifs, whereas more heterogeneous local arrangements produce a broader distribution of configurations. Rather than evaluating this entropy at a single recurrence threshold, we systematically vary the threshold and examine the resulting entropy profile, probing how the diversity of local recurrence configurations changes as the recurrence criterion is relaxed. The threshold corresponding to the maximum entropy is then selected as the representative threshold, together with its associated entropy value, providing a compact descriptor of the spatial pattern [30]. From this dependence, we extract characteristic entropy and threshold values that provide compact descriptors of the spatial pattern.

Several approaches have been developed to characterize spatial patterns, each emphasizing different aspects of spatial organization. Statistical descriptors based on gray-level distributions and co-occurrence matrices provide measures such as contrast, homogeneity, and correlation [31], while Fourier and wavelet methods characterize spectral and multiscale properties [32]. Geometrical descriptors, including fractal dimension and lacunarity, quantify self-similarity, roughness, and scale-dependent organization [33, 34]. Machine learning and deep learning methods have also achieved remarkable performance in image classification and segmentation, particularly when large annotated datasets are available [13, 35, 36]. These approaches provide powerful and complementary descriptions, but their sensitivity to specific spatial properties, representations, or training procedures motivates the development of additional descriptors based directly on spatial configurations.

Information-theoretic approaches offer a complementary perspective by quantifying statistical organization and uncertainty without requiring a specific model for the underlying system. Since the seminal work of Shannon [37], entropy-based measures have been widely applied to signal and image analysis [38, 39], with permutation entropy providing a simple and robust framework for extracting information from the

ordinal structure of data [40]. In this context, recurrence plots provide a natural framework for describing relationships between local configurations. Originally introduced by Eckmann *et al.* [41] for the visualization of recurrences in phase-space trajectories, recurrence plots were later complemented by recurrence quantification analysis (RQA) [42, 43]. Their use was subsequently extended to spatially distributed systems and images, including spatial recurrence plots [44], generalized recurrence plots and generalized recurrence quantification analysis [45]. Spatial recurrence measures have been used to characterize Turing patterns and to identify structural changes and dynamical regimes in reaction-diffusion systems [46, 47].

Despite these developments, recurrence-based descriptions generally require the recurrence threshold to be fixed or selected according to a prescribed criterion before recurrence measures are evaluated. The threshold therefore determines which configurations are considered recurrent, but its dependence has rarely been explored as a source of information about the spatial organization of a pattern itself [30, 48]. Here, we investigate whether the variation of recurrence entropy across threshold values can provide additional information about spatial structure. Because recurrence motifs are defined from local relationships between neighboring pixels, spatial variations in these relationships are expected to modify the distribution of motifs. Thus, interfaces, boundaries, local heterogeneities, and regions with different degrees of spatial organization can be reflected in the statistical composition of recurrence configurations. This provides a basis for testing the sensitivity of recurrence entropy to different forms of spatial structure and for assessing whether its threshold dependence provides a meaningful descriptor of pattern organization.

To this end, we evaluate the framework using four complementary classes of spatial patterns: fractional Brownian surfaces, Turing patterns, Voronoi tessellations, and textures from the Kylberg dataset. Typical examples are shown in Fig. 1. These patterns were selected to probe distinct aspects of spatial organization. Fractional Brownian surfaces provide controlled variations in spatial correlations and roughness, Turing patterns exhibit organized structures and characteristic spatial scales, Voronoi tessellations provide a controlled geometry with systematically varying interfaces and spatial heterogeneity, and the Kylberg textures provide real-world examples with diverse local organizations. Together, these datasets allow us to test whether recurrence entropy responds systematically to controlled changes in spatial structure and whether the resulting entropy profiles provide a compact description of qualitatively different patterns.

2 Results

2.1 $\bar{S} \times \bar{\delta}$: a diagram for characterization of spatial patterns

2.1.1 Fractional Brownian Surfaces

To test the sensitivity of the proposed descriptors to controlled variations in spatial correlation, we first consider fractional Brownian surfaces, whose spatial organization can be systematically varied through the Hurst exponent H. Figure 2 shows the results

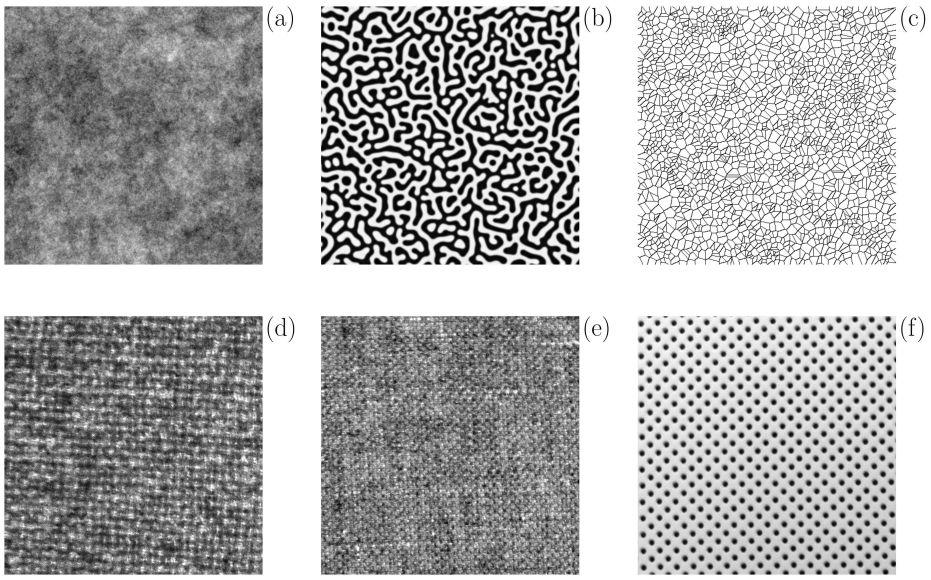


Fig. 1 Examples of the spatial patterns analyzed in this study. The first row shows synthetic patterns: (a) fractional Brownian surface, (b) Turing pattern, and (c) Voronoi tessellation. The second row shows three examples from the Kylberg texture dataset: (d) blanket, (e) canvas, and (f) ceiling 2.

for the Brownian surfaces generated on a 1024×1024 grid, with pixel values normalized between 0 and 1. The results are presented as error bars corresponding to the mean value plus or minus one standard deviation, computed from 100 independent realizations. Each color represents a different Hurst exponent, with H values ranging from 0 to 1 in steps of 0.1 (see Sec. 4.2.1 for details). In panel (a), we plot the representative entropy $\bar{S}$, as defined in Eq. (4), as a function of H and observe a decreasing trend as H increases. This behavior is consistent with the increasing spatial correlation of surfaces with higher Hurst exponents, which leads to more spatially organized structures. In panel (b), we show the corresponding threshold $\bar{\delta}$, defined in Eq. (5), as a function of H, which also exhibits a monotonic decrease. In panel (c), we present the average recurrence rate $\langle \varrho \rangle$, as defined in Eq. (7). As discussed in [49], distinguishing between surfaces with low Hurst exponents can be challenging, particularly when using entropy-based measures. Finally, in panel (d), we present the $(\bar{S}, \bar{\delta})$ diagram. The data points are more evenly distributed in this representation, facilitating the visual distinction between surfaces generated with different H values.

2.1.2 Turing Patterns

To assess the sensitivity of the proposed descriptors to organized spatial structures and characteristic pattern scales, we next consider Turing patterns with different morphologies and characteristic sizes. Figure 3 shows the $\bar{S} \times \bar{\delta}$ (a) and $\langle \varrho \rangle \times \bar{\delta}$ (b) diagrams for the four distinct Turing patterns generated using Eqs. (8) and (9) (see Sec. 4.2.2 for details). The error bars represent one standard deviation from the mean, calculated

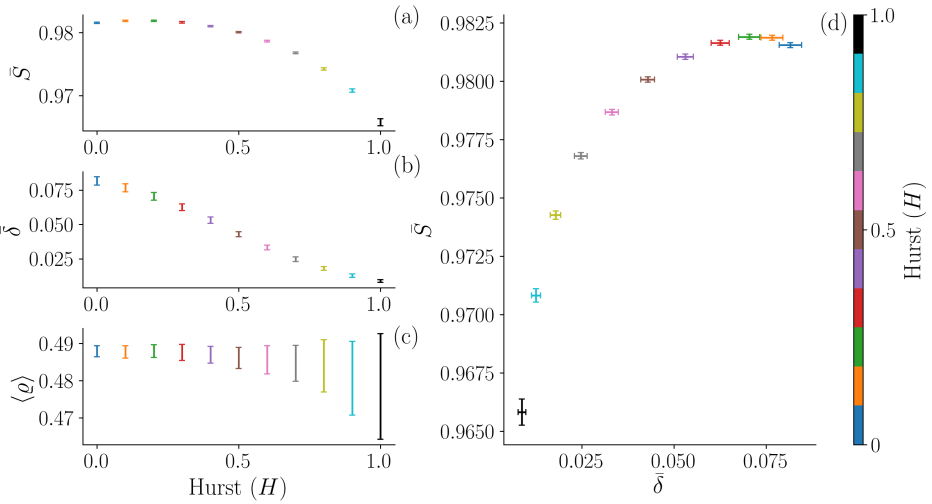


Fig. 2 Quantitative analysis of Brownian surfaces with distinct Hurst exponents $H \in [0, 1]$ in steps of 0.1, generated as described in Sec. 4.2.1. Each point represents the average value over 100 realizations on a 1024×1024 grid with pixel intensities normalized between 0 and 1. Panel (a) shows the entropy $\bar{S}$ as a function of H, and panel (b) presents the dissimilarity index $\bar{\delta}$ versus H, both exhibiting a decreasing trend with increasing H. Panel(c) displays the average recurrence rate $\langle\varrho\rangle$ as a function of H. Panel (d) displays the $(\bar{S}, \bar{\delta})$ diagram, where the measures provide a clearer separation between surfaces generated with different H values. Error bars correspond to one standard deviation.

over 100 independent realizations. The two representations separate the different patterns in the feature space. Notably, similar values of $\bar{S}$ do not necessarily correspond to similar spatial structures, as differences in $\bar{\delta}$ provide an additional dimension for distinguishing the patterns. In particular, panel (a) shows that patterns with different characteristic sizes occupy distinct regions of the $(\bar{S}, \bar{\delta})$ space. Larger circular and stripe patterns are associated with lower values of both $\bar{S}$ and $\bar{\delta}$, whereas smaller patterns occupy regions characterized by higher values of these quantities. This behavior can be related to the spatial organization of the patterns: as the characteristic size of the structures decreases, the number of interfaces and local spatial variations increases throughout the image. Consequently, a greater diversity of local recurrence configurations is observed, leading to a broader distribution of recurrence motifs and higher entropy values. These results indicate that recurrence entropy is sensitive not only to the morphology of the patterns but also to their characteristic spatial scale.

2.1.3 Kylberg Dataset

To assess the behavior of the proposed descriptors on real-world textures, we finally consider the Kylberg dataset, which provides a more challenging test due to the greater variability and complexity of naturally occurring spatial structures. Figure 4 presents the $\bar{S} \times \bar{\delta}$ (a) and $\langle\varrho\rangle \times \bar{\delta}$ (b) diagrams obtained for the Kylberg dataset (see Sec. 4.2.3 for details). Since the pixel intensities are discrete integer values ranging from 0 to 255, the recurrence threshold δ was varied in integer steps within this interval. The resulting diagrams show that different texture patterns tend to occupy distinct regions of the

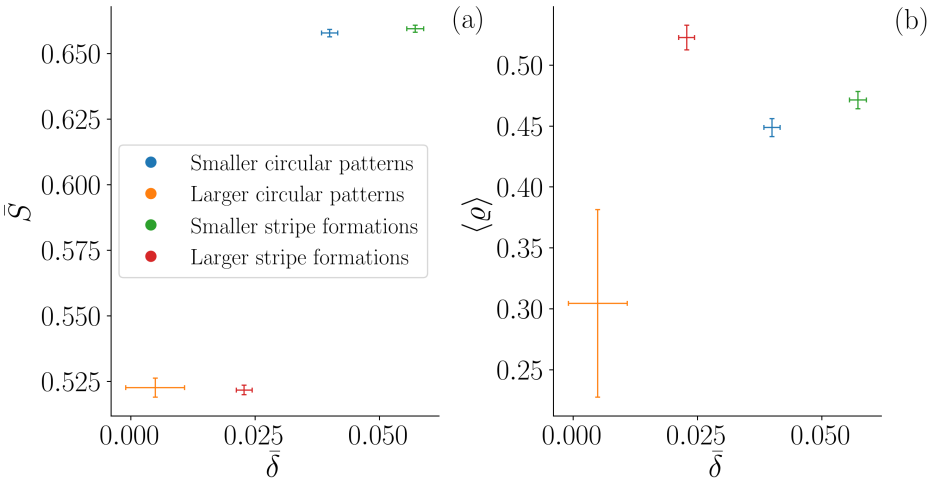


Fig. 3 (a) $\bar{S} \times \bar{\delta}$ and (b) $\langle \varrho \rangle \times \bar{\delta}$ diagrams, for the four distinct turning patterns generated as described in Sec. 4.2.2. The error bars correspond to one standard deviation over 100 distinct realizations of the spatial patterns.

feature space, indicating that recurrence-based descriptors are sensitive to their underlying spatial organization. The separation is particularly evident in the $\bar{S} \times \bar{\delta}$ plane. Although some overlap is observed for textures with similar visual appearance, many texture types form relatively well-defined regions characterized by distinct entropy and threshold values. This behavior suggests that recurrence entropy captures differences in local spatial arrangements and texture organization. In contrast, the $\langle \varrho \rangle \times \bar{\delta}$ plane exhibits substantially greater overlap. Although the recurrence rate still reflects variations in local texture organization, its smaller dynamic range provides less separation between the different patterns. These results indicate that recurrence entropy provides information beyond the overall recurrence rate, with the pair $(\bar{S}, \bar{\delta})$ offering a richer representation of spatial texture organization.

2.2 Sensitivity to Spatial Scale in Voronoi Tessellations

To investigate the sensitivity of recurrence entropy to spatial scale, we analyzed ensembles of binary Voronoi tessellations generated from randomly distributed seeds (see Sec. 4.2.4). In contrast to the previous datasets, which were primarily employed for pattern characterization, Voronoi tessellations provide a controlled framework in which the characteristic spatial scale can be modified while maintaining a fixed image resolution. For each realization, a set of (N_s) seeds was randomly distributed over a (512×512) domain and the corresponding Voronoi tessellation was constructed. Only the cell boundaries were retained, yielding binary images in which boundary pixels assume value one and all remaining pixels assume value zero. Since the images are binary, the recurrence analysis was performed using $(\delta = 0)$, such that two pixels were considered recurrent only when their values were identical.

For each value of N_s, one hundred independent realizations were generated and the corresponding recurrence entropy was computed. Figure 5 presents the resulting

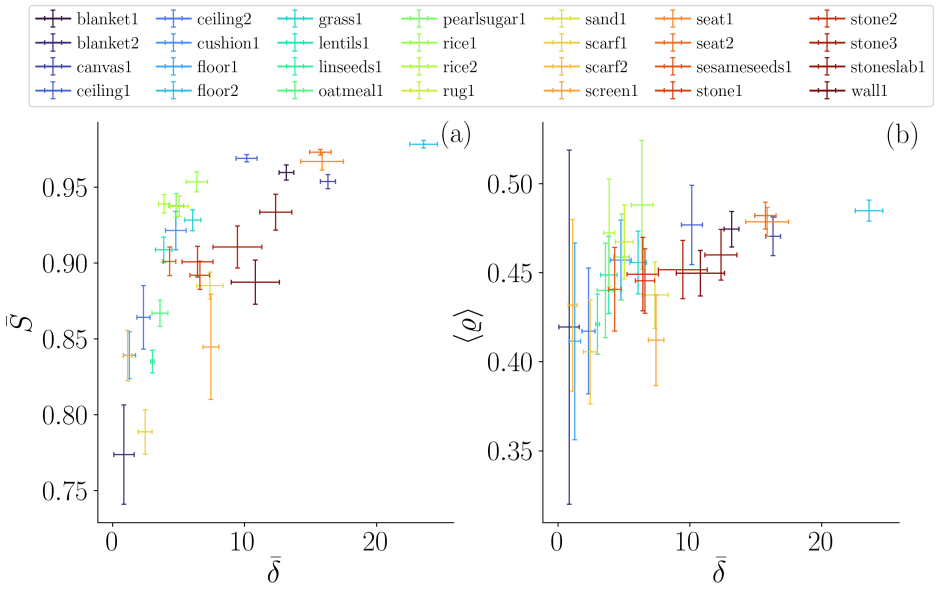


Fig. 4 $\bar{S} \times \bar{\delta}$ (a) and $\langle \varrho \rangle \times \bar{\delta}$ (b) diagrams for the Kylberg dataset. The recurrence threshold δ is varied in integer steps from 0 to 255. The texture classes are generally well-separated, with minor overlaps for a few classes.

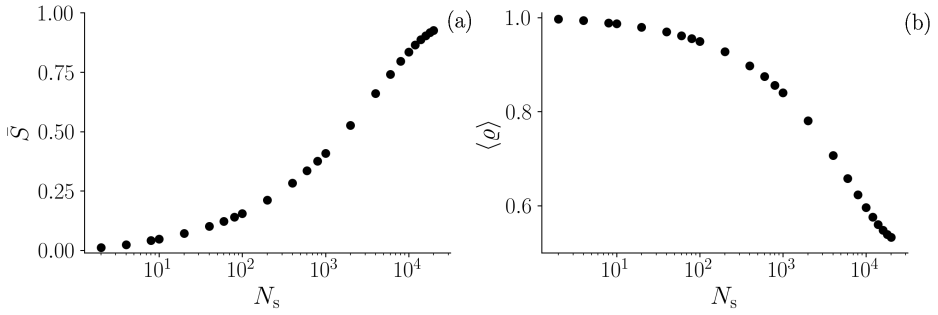


Fig. 5 (a) Mean recurrence entropy $\bar{S}$ and (b) average recurrence rate $\langle \varrho \rangle$ as a function of the number of Voronoi seeds N_s. Increasing N_s reduces the characteristic cell size while maintaining a fixed image resolution (512×512), revealing the sensitivity of recurrence entropy to progressively finer spatial scales.

dependence of recurrence entropy (panel a) and the average recurrence rate (panel b) on the number of seeds. Error bars corresponding to one standard deviation are omitted because their magnitude is negligible on the scale of the plots. As the number of seeds increases, the characteristic size of the Voronoi cells decreases approximately as $\ell \sim L/\sqrt{N_s}$ [50], leading to a progressive increase in the density of interfaces and junctions within the image. Consequently, the spatial organization becomes increasingly structured across smaller scales while the total number of pixels remains unchanged.

A clear monotonic increase in recurrence entropy, accompanied by a decrease in the average recurrence rate, is observed as the number of seeds (N_s) increases. Since the image resolution is fixed throughout the analysis, this variation reflects changes in spatial organization rather than image size or sampling density. As N_s increases, the characteristic size of the Voronoi cells decreases, leading to a higher density of interfaces and junctions and, consequently, to a greater diversity of local recurrence configurations. This behavior is consistent with the results obtained for the Turing patterns (see Fig. 3), where structures with smaller characteristic spatial scales also exhibit higher entropy values. Taken together, these results indicate that recurrence entropy is sensitive to the characteristic spatial scale of a pattern. The Voronoi benchmark therefore provides a controlled framework that the measure can capture changes in geometric organization and coarse-graining even when image resolution and grayscale intensity remain unchanged.

3 Conclusions

In this work, we introduced a recurrence-based framework for the characterization of spatial patterns by extending concepts from recurrence analysis to two-dimensional pattern data. The proposed approach relies on the construction of recurrence motifs and the computation of recurrence entropy, providing a compact representation of spatial organization through the joint analysis of the recurrence threshold and its associated entropy. The methodology was validated using synthetic datasets, including fractional Brownian surfaces and Turing patterns, as well as real-world textures from the Kylberg dataset. Across these systems, recurrence entropy proved capable of distinguishing different classes of patterns and capturing structural variations associated with changes in spatial correlations.

The results highlight both the strengths and limitations of the proposed framework. On the positive side, recurrence entropy provides an interpretable and computationally simple descriptor that can be applied to synthetic, experimental, and real-world datasets within a unified framework. Furthermore, the Voronoi tessellation analysis show that the method is sensitive to variations in characteristic spatial scale, revealing systematic entropy changes as increasingly fine geometric structures are introduced while maintaining a fixed image resolution. On the other hand, the sensitivity of the entropy measure depends on the underlying image structure, with some highly organized patterns exhibiting relatively small entropy variations. Consequently, recurrence entropy should be used as a diagnostic tool that captures some aspects of spatial pattern organization, complementing the information provided by other complexity indicators.

Several directions for future research remain open. A natural extension is the systematic investigation of robustness against different noise sources and noise intensities. The framework may also be generalized to color and multi-channel images, enabling applications beyond grayscale texture analysis. In addition, the use of two recurrence thresholds, ($\delta_{\min}$) and ($\delta_{\max}$), could provide a mechanism for selecting specific intensity ranges and isolating relevant spatial structures from either original or preprocessed images. Such developments may further enhance the ability of recurrence-based

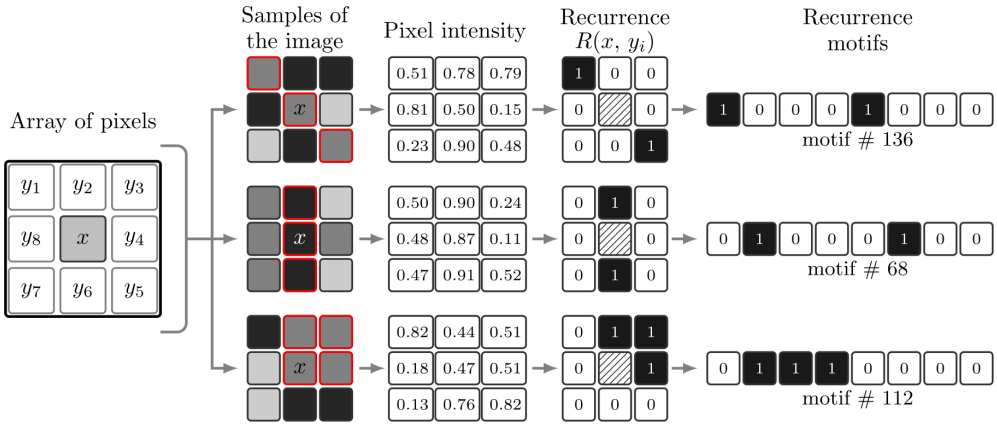


Fig. 6 Illustration of the recurrence motif construction. The left panel shows the eight-connected neighborhood of a central pixel x, surrounded by its neighboring pixels $y_1, \ldots, y_8$. The three examples on the right illustrate the construction of recurrence motifs from different local intensity configurations. For each example, the grayscale pixel values are compared with the central pixel according to the recurrence threshold δ, generating eight binary recurrence relations $R(x, y_i)$. The red border indicates recurrent pixels. The resulting binary configuration defines the corresponding recurrence motif, shown on the right. Here, the recurrence threshold is fixed at $\delta = 0.05$ for illustration; changing δ may modify the recurrence relations and, consequently, the resulting motifs.

descriptors to extract multiscale information and reveal hidden structural features in complex spatial datasets.

4 Methods

4.1 Recurrence motifs and entropy

To quantify the spatial complexity of the patterns analyzed in our study, we introduce a local entropy measure based on recurrence motifs. The method is applied to grayscale patterns represented as two-dimensional arrays of size $N \times M$, where each pixel at position (i, j) is associated with a single scalar value $I(i, j)$, hereafter referred to as the pixel intensity. Depending on the dataset, this intensity may be represented either by a discrete integer value, such as in standard 8-bit grayscale images, or by a continuous real-valued quantity obtained from numerical simulations or experimental measurements. The proposed framework is independent of the numerical representation and can therefore be applied to both discrete and continuous patterns. For each non-border pixel x, we consider its eight-connected neighborhood, composed of its immediate neighboring pixels $y_1, \ldots, y_8$, as illustrated in Fig. 6. For a prescribed recurrence threshold δ, the intensity of the central pixel is compared with that of each neighboring pixel, and a recurrence relation is assigned according to the thresholded similarity criterion [41]:

$$R(x, y_i) = \Theta\left(\delta - |I(x) - I(y_i)|\right), \qquad i = 1, \cdots, 8, \tag{1}$$

where $I(\cdot)$ denotes the scalar intensity associated with a pixel, $\Theta(\cdot)$ is the Heaviside function, and δ is the recurrence threshold. Thus, each neighborhood gives rise to eight binary recurrence relations, as illustrated by the three examples in Fig. 6. The resulting ordered binary configuration defines the recurrence motif associated with the central pixel:

$$n(x) = [R(x, y_1),\ R(x, y_2),\ \ldots,\ R(x, y_8)]. \tag{2}$$

Since each entry in the motif vector is binary, there are $2^8 = 256$ possible distinct motifs. Since the recurrence motifs are defined from local relationships between neighboring pixels, their distribution is expected to reflect the spatial organization of the pattern. Different spatial arrangements can give rise to distinct sets of local recurrence configurations. For example, elongated structures with predominantly vertical interfaces may produce recurrence motifs with different frequencies from those generated by circular or isotropic structures. Likewise, changes in the characteristic size of the structures can modify the relative amount of interior and boundary regions. As the number and spatial distribution of interfaces change, the local recurrence relations between neighboring pixels are correspondingly altered, leading to changes in the statistical distribution of recurrence motifs. Thus, the motif distribution provides a direct link between local spatial organization and the frequency of occurrence of each motif. It is important to note that the proposed methodology is invariant under 90° rotations of the image and under inversion of the pixel intensities, i.e., exchanging black and white.

We iterate through all non-border pixels in the image to construct a distribution $P(m)$ over the observed motifs m. Finally, we compute the Shannon entropy of the motif distribution:

$$S(\delta) = -\sum_{m} P(m) \log P(m), \tag{3}$$

where the sum is taken over all motifs with non-zero probability, this entropy value $S(\delta)$ provides a quantitative measure of the spatial complexity of the image, ranging from 0 to $\log(256) = 8$. To facilitate comparison across different patterns and parameter settings, we normalize the entropy by dividing by its maximum possible value, yielding a dimensionless quantity between 0 and 1.

A critical step in recurrence-based analyses is the selection of the recurrence threshold (δ), which determines whether two states are considered recurrent. The threshold directly controls the density of recurrence points in the recurrence matrix and therefore strongly influences the distribution of recurrence motifs and the resulting entropy values. If δ is chosen too small, only a limited number of recurrences are detected, whereas excessively large values may lead to an almost fully recurrent matrix, reducing the discriminative power of the analysis [43, 51]. Consequently, the choice of δ remains one of the most important practical issues in recurrence quantification analysis.

Several strategies have been proposed to select suitable threshold values, including fixed recurrence rates, distance-based criteria, and heuristic percentages of the phase-space diameter [43, 51]. In the present work, rather than fixing δ to a single value, we systematically investigate how the recurrence entropy varies with the recurrence threshold. For a given pattern, the entropy is evaluated over a range of thresholds, yielding the entropy curve $S(\delta)$. This curve provides additional information about the statistical organization of the patterns. In particular, different patterns may exhibit

distinct entropy profiles, reflecting differences in the distribution of pixel intensities and local spatial arrangements. Therefore, the threshold itself becomes an additional source of information that can be exploited for pattern characterization.

For applications focused on pattern classification and state characterization, we follow the entropy maximization approach proposed in [30]. In this case, the representative entropy of the image is defined as

$$\bar{S} = \max_{\delta} S(\delta), \tag{4}$$

which occurs at a corresponding threshold value $\bar{\delta}$. Thus, $\bar{\delta}$ is defined as the threshold value that maximizes the recurrence entropy,

$$\bar{\delta} = \arg\max_{\delta} S(\delta). \tag{5}$$

This threshold is subsequently used to characterize the representative entropy of the pattern. The rationale behind this approach is that the entropy reaches its maximum when the diversity of recurrence motifs is largest, indicating the threshold that reveals the richest set of local spatial configurations present in the patterns. Inspired by the feature extraction framework proposed in [52], the pair $(\bar{S}, \bar{\delta})$ can be interpreted as a compact descriptor of the patterns. Different spatial patterns tend to occupy distinct regions in the $(\bar{S}, \bar{\delta})$ plane, providing a simple and interpretable feature space for characterization and classification.

To illustrate the influence of the recurrence threshold on entropy estimation, Fig. 7 presents two artificially generated images composed of independent random pixels. Panel (a) shows an image generated from a uniform distribution and panel (b) an image generated from a normal distribution. In both cases, pixel intensities are real-valued and normalized between 0 and 1. Although both patterns are generated from random processes, the distinct probability distributions of pixel intensities lead to markedly different entropy curves $S(\delta)$, shown in panel (c). The uniform distribution reaches a maximum entropy of $\bar{S} = 0.997$ at $\bar{\delta} = 0.29$, whereas the normal distribution reaches $\bar{S} = 0.977$ at $\bar{\delta} = 0.10$. These example expose that both the entropy and the threshold associated with its maximum contain useful information regarding the underlying statistical properties of the image. Consequently, the entropy curve $S(\delta)$ provides a natural framework for exploring spatial complexity across different scales of similarity.

In association with $\bar{S}$ and $\bar{\delta}$, we proceed to extract additional information from the recurrence patterns of each pixel. One such feature is the local recurrence rate, which quantifies the proportion of neighboring pixels that are recurrent to a given central pixel. For a pixel located at position x, the local recurrence rate ϱ_x is defined as

$$\varrho_x = \frac{1}{8} \sum_{i=1}^{8} R(x, y_i), \tag{6}$$

where $R(x, y_i)$ is the binary recurrence between the pixel x and its i-th neighbor y_i. This measure captures the local homogeneity of a pixel's neighborhood: a value

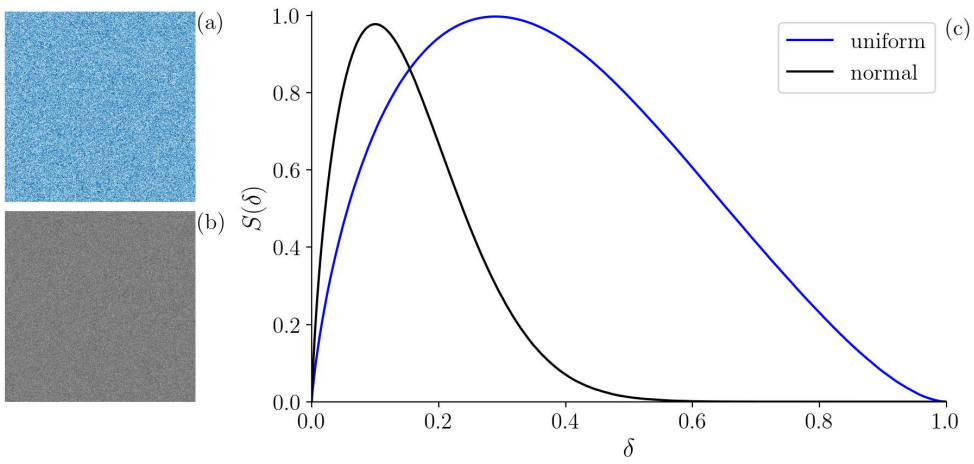


Fig. 7 Artificially generated patterns using uniform (a, blue scale) and normal (b, gray scale) distributions for 512×512 pixels created with values from 0 to 1, and corresponding entropy curves $S(\delta)$ as a function of the threshold δ (c). Despite being purely noisy, differences in pixel intensity distributions lead to distinct entropy profiles, with the uniform case peaking at $\bar{S} = 0.997$ for $\bar{\delta} = 0.29$ and the normal case at $\bar{S} = 0.977$ for $\bar{\delta} = 0.1$.

of $\varrho_x = 1$ indicates full recurrence (i.e., all neighbors are recurrent), while $\varrho_x = 0$ indicates the absence of any recurrence. Based on the local recurrence rates, it is also possible to compute the average recurrence rate across the image, defined as:

$$\langle \varrho \rangle = \frac{1}{(N-2)(M-2)} \sum_{j=2}^{N-1} \sum_{k=2}^{M-1} \varrho_{j,k}, \tag{7}$$

where $\varrho_{j,k}$ represents the local recurrence rate of the pixel at position (j, k), and the summation excludes the border pixels to ensure all neighborhoods are fully defined. This global quantity reflects the overall level of recurrence or homogeneity in the patterns, and can serve as an additional feature for texture characterization.

4.2 Dataset

4.2.1 Fractional Brownian surfaces

Fractional Brownian surfaces (fBs) are stochastic self-affine fields characterized by long-range spatial correlations governed by the Hurst exponent $H \in (0, 1)$ [53]. They constitute a two-dimensional extension of fractional Brownian motion and have been widely employed to model natural textures, rough surfaces, geophysical landscapes, and heterogeneous media [54]. The Hurst exponent controls both the roughness and correlation structure of the surface: small values of H generate highly irregular patterns with weak spatial persistence, whereas large values of H produce smoother structures

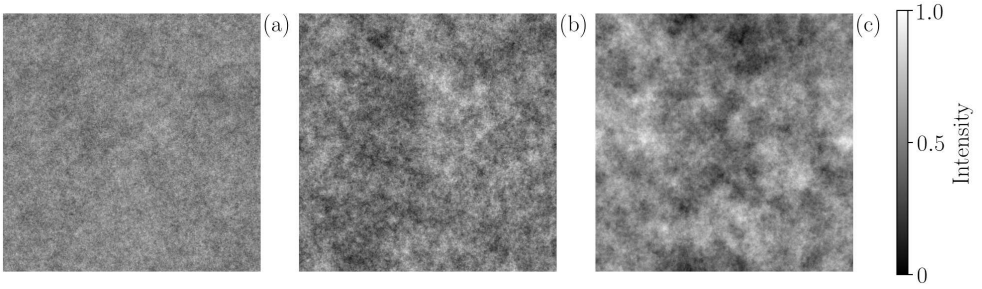


Fig. 8 Artificially generated fractional Brownian surfaces (fBs) for 1024×1024 pixels for distinct Hurst exponents of generation (H): (a) $H = 0.2$, (b) $H = 0.5$, and (c) $H = 0.8$. The larger the parameter, the smoother the surface.

with stronger long-range correlations. Figure 8 illustrates three representative realizations of fractional Brownian surfaces of size 1024×1024 generated with different Hurst exponents: (a) $H = 0.2$, (b) $H = 0.5$, and (c) $H = 0.8$.

4.2.2 Turing Patterns

Alan Turing showed that simple reaction–diffusion mechanisms can generate complex spatial structures, providing a theoretical explanation for patterns such as stripes and spots observed in nature [55]. Reaction–diffusion systems describe the spatiotemporal evolution of interacting chemical species through local reactions and diffusion processes. In this work, we employ a classical two-species reaction–diffusion model, inspired by the implementation presented in [56], to generate artificial spatial patterns. The dynamics are governed by the concentrations ($u(x, y, t)$) and ($v(x, y, t)$), whose evolution is described by

$$\frac{\partial u}{\partial t} = D_u \nabla^2 u + F_u(u, v) \tag{8}$$

$$\frac{\partial v}{\partial t} = D_v \nabla^2 v + F_v(u, v) \tag{9}$$

where D_u and D_v are the diffusion coefficients, and $F_u(u, v) = u - u^3 - v + \alpha$ and $F_v(u, v) = (u - v)\beta$ describe the local reaction kinetics between the two components. The first term in each equation accounts for spatial diffusion, while the second term models local interactions such as production, inhibition, or decay. Under appropriate conditions, this coupling between diffusion and reaction can destabilize a homogeneous steady state, forming spatially organized structures known as Turing patterns.

Figure 9 illustrates spatial patterns generated by a reaction-diffusion system (Eqs. (8, 9)). The grid composed of 512×512 points is initialized with random concentrations of the u and v, and the system evolves for 500 steps, with each step involving 100 updates. The final pattern of $u(x, y)$ is displayed in grayscale, where darker areas indicate lower concentrations of species u and lighter areas indicate higher concentrations. Panel (a) displays a pattern consisting of small, circular formations. Panel (b)

shows a pattern with larger circular formations. Panel (c) presents smaller, stripe-like structures, while panel (d) illustrates larger stripe formations.

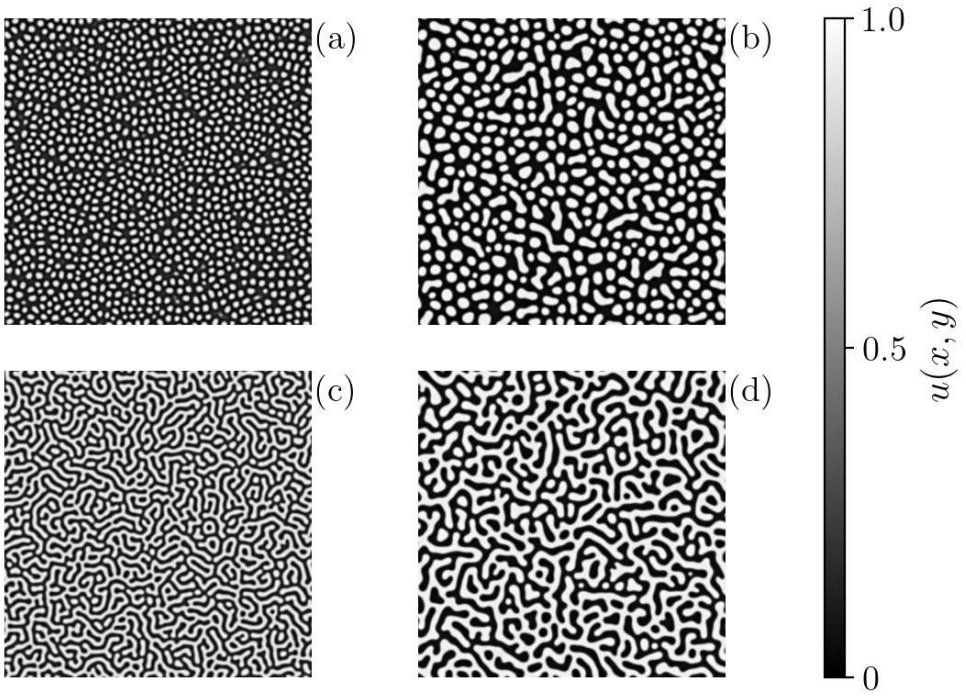


Fig. 9 Turing patterns generated by a reaction-diffusion system [Eqs. (8 - 9)]. Panel (a) shows small circular formations $D_u = 1$, $D_v = 100$, $\alpha = -0.05$, and $\beta = 10$, (b) displays larger circles $D_u = 1$, $D_v = 200$, $\alpha = -0.1$, and $\beta = 2$, (c) presents smaller stripes $D_u = 1$, $D_v = 100$, $\alpha = -0.001$, and $\beta = 10$, and (d) illustrates larger stripes $D_u = 1$, $D_v = 200$, $\alpha = 0.5$, and $\beta = 2$.

4.2.3 Kylberg Dataset

The Kylberg Dataset, consists of 28 distinct texture classes. Each class includes 160 multiple grayscale images captured under controlled conditions to ensure consistency in scale and illumination. The textures represent a variety of natural surfaces, providing a diverse set of patterns for classification and analysis. The images are preprocessed to highlight texture characteristics while minimizing background noise. Figure 10 illustrates the first sample of each class. The dataset is free and it's available in [57].

4.2.4 Synthetic Voronoi Patterns

To further investigate the sensitivity of the proposed recurrence entropy to spatial scale, we considered a family of synthetic patterns based on Voronoi tessellations.

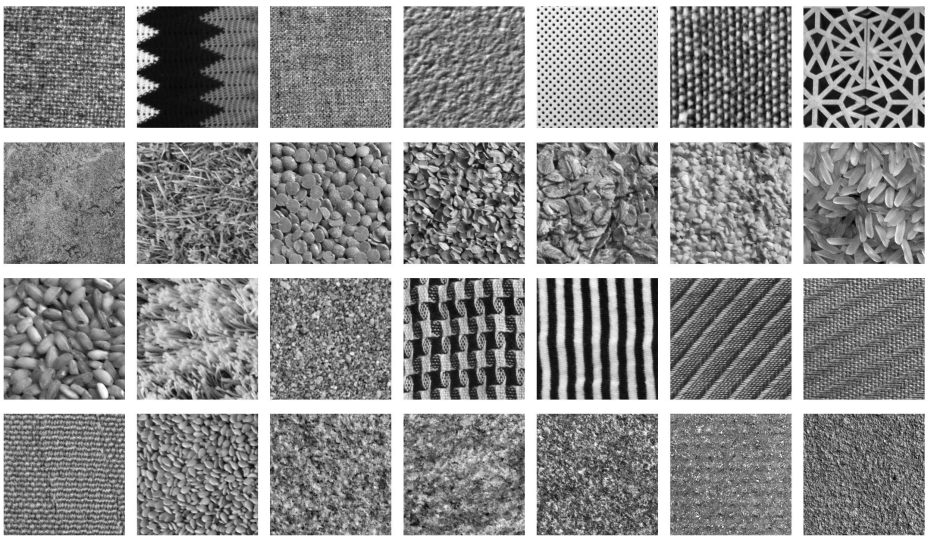


Fig. 10 The first sample of each of the 28 classes of the Kylberg Dataset [57].

Voronoi patterns provide a controlled framework in which the characteristic spatial scale can be systematically modified while maintaining a fixed image resolution. A Voronoi tessellation is generated from a set of N_s seed points randomly distributed over a two-dimensional domain. Each pixel is assigned to the nearest seed according to the Euclidean distance, partitioning the image into a collection of polygonal regions known as Voronoi cells [50].

In the present work, images of size 512×512 pixels were generated by randomly placing N_s seeds in the domain. After constructing the Voronoi tessellation, only the cell boundaries were retained, producing binary images in which pixels belonging to a boundary assume value one and all remaining pixels assume value zero. This representation emphasizes the geometric organization of the tessellation and allows the recurrence analysis to focus exclusively on the spatial arrangement of interfaces. Increasing N_s introduces progressively finer spatial structures while preserving the overall image dimensions. In this sense, the number of seeds acts as a control parameter governing the characteristic observation scale of the pattern. Figure 11 presents representative realizations generated for different numbers of seeds. As the number of seeds increases, the characteristic size of the Voronoi cells decreases, leading to a larger number of interfaces within the same image domain.

Acknowledgements. Conselho Nacional de Desenvolvimento Científico e Tecnológico (CNPq), Grants Nos. 300281/2026-9 (SRL), 407072/2022-5 (SRL), 443575/2024-0 (SRL), 305189/2022-0 (TLP), 408254/2022-0 (TLP), 318849/2025-9 (TLP), and the INCT-NeuroComp (CNPq Grant Nos. 408389/2024-9 (TLP) and 150376/2026-0 (BRRB)); Coordenação de Aperfeiçoamento de Pessoal de Nível Superior (CAPES), Grants Nos. 88881.895032/2023-01 (SRL) and 88881.189166/2025-01 (TLP), and Finance Code 001. B.R.R.B and E.E.N.M. are supported by the Brazilian

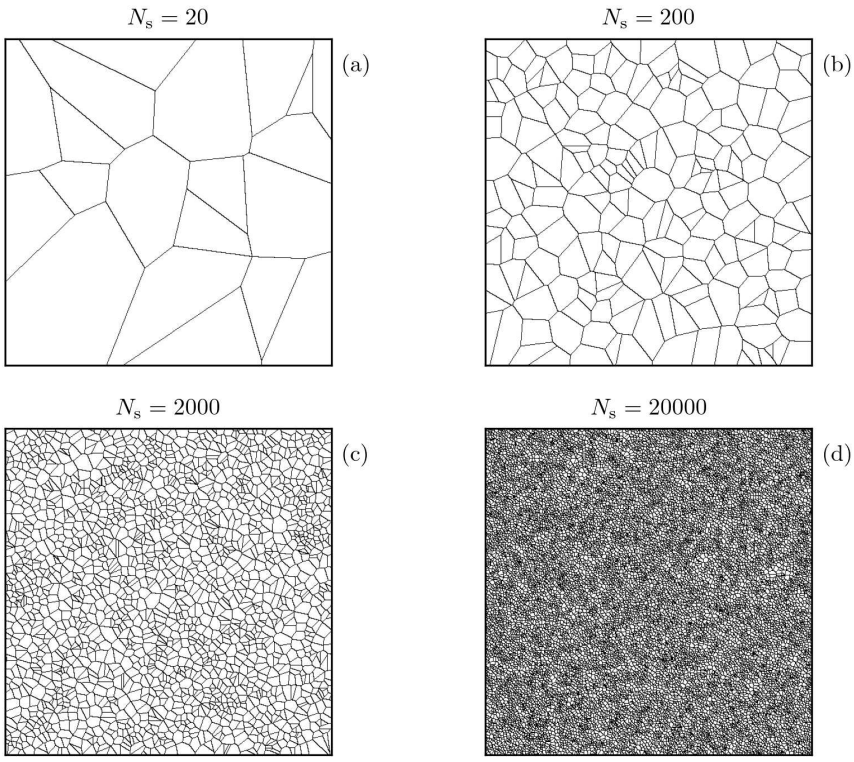


Fig. 11 Representative Voronoi tessellations generated using: (a) $N_s = 20$, (b) 200, (c) 2000, and (d) 20000 seeds. Only the cell boundaries are displayed, resulting in binary images. Increasing the number of seeds decreases the characteristic cell size and increases the density of interfaces and vertices, providing a controlled mechanism to investigate the sensitivity of recurrence entropy to spatial scale while maintaining a fixed image resolution.

São Paulo Research Foundation (FAPESP), Proc. 2021/09839-0, 2023/16273-8, and 2024/05700-5 — "Dinâmica Não Linear". C.M. acknowledges the support of project PID2024-160573NB-I00 funded by MICIU/AEI/10.13039/501100011033 and FEDER, UE.

Data availability

The code and supporting materials used in this study are available in the GitHub repository at (github.com). The Kylberg Texture Dataset v. 1.0, used in this study, is publicly available at https://user.it.uu.se/~gusky180/texture/. The dataset is maintained by its original author and is not part of the authors' GitHub repository.

References

[1] Zhao, L., Macau, E.E.N.: A network of dynamically coupled chaotic maps for

scene segmentation. IEEE Transactions on Neural Networks **12**(6), 1375–1385 (2001)

[2] Prado, T.L., Galuzio, P.P., Lopes, S.R., Viana, R.L.: Spatial recurrence analysis: A sensitive and fast detection tool in digital mammography. Chaos: An Interdisciplinary Journal of Nonlinear Science **24**(1) (2014)

[3] Kather, J.N., Weis, C., Bianconi, F., Melchers, S.M., Schad, L.R., Gaiser, T., Marx, A., Zöllner, F.G.: Multi-class texture analysis in colorectal cancer histology. Scientific Reports **6**(1), 27988 (2016)

[4] Giuliani, G., Dao, H., De Bono, A., Chatenoux, B., Allenbach, K., De Laborie, P., Rodila, D., Alexandris, N., Peduzzi, P.: Live Monitoring of Earth Surface (LiMES): A framework for monitoring environmental changes from Earth Observations. Remote Sensing of Environment **202**, 222–233 (2017)

[5] Rietkerk, M., Bastiaansen, R., Banerjee, S., Koppel, J., Baudena, M., Doelman, A.: Evasion of tipping in complex systems through spatial pattern formation. Science **374**(6564), 0359 (2021)

[6] Yuan, X., Shi, J., Gu, L.: A review of deep learning methods for semantic segmentation of remote sensing imagery. Expert Systems with Applications **169**, 114417 (2021)

[7] Merchant, A., Batzner, S., Schoenholz, S.S., Aykol, M., Cheon, G., Cubuk, E.D.: Scaling deep learning for materials discovery. Nature **624**(7990), 80–85 (2023)

[8] Ge, Z.: The hidden order of turing patterns in arid and semi-arid vegetation ecosystems. Proceedings of the National Academy of Sciences **120**(42), 2306514120 (2023)

[9] Singh, Y., Farrelly, C.M., Hathaway, Q.A., Leiner, T., Jagtap, J., Carlsson, G.E., Erickson, B.J.: Topological data analysis in medical imaging: current state of the art. Insights into Imaging **14**(1), 58 (2023)

[10] Ramos, R., Swedlund, B., Ganesan, A.K., Morsut, L., Maini, P.K., Monuki, E.S., Lander, A.D., Chuong, C., Plikus, M.V.: Parsing patterns: Emerging roles of tissue self-organization in health and disease. Cell **187**(13), 3165–3186 (2024)

[11] Soltisz, A.M., Craigmile, P.F., Veeraraghavan, R.: Spatial pattern analysis using closest events (SPACE) — a nearest neighbor point pattern analysis framework for assessing spatial relationships from digital images. Microscopy and Microanalysis **30**(2), 306–317 (2024)

[12] Omarzadeh, D., González-Godoy, A., Bustos, C., Martín-Fernández, K., Scotto, C., Sánchez, C., Lapedriza, A., Borge-Holthoefer, J.: Explainable automatic detection of fiber–cement roofs in aerial RGB images. Remote Sensing **16**(8),

1342 (2024)

[13] Sindhura, D.N., Pai, R.M., Bhat, S.N., Pai, M.M.M.: A review of deep learning and generative adversarial networks applications in medical image analysis. Multimedia Systems **30**(3), 161 (2024)

[14] Medghalchi, S., Kortmann, J., Lee, S., Karimi, E., Kerzel, U., Korte-Kerzel, S.: Automated segmentation of large image datasets using artificial intelligence for microstructure characterisation and damage analysis. Materials & Design **243**, 113031 (2024)

[15] Mgohele, R.N., Massawe, B.H.J., Shitindi, M.J., Sanga, H.G., Omar, M.M.: Prediction of soil texture using remote sensing data. a systematic review. Frontiers in Remote Sensing **5**, 1461537 (2024)

[16] Liboni, L.H.B., Budzinski, R.C., Busch, A.N., Löwe, S., Keller, T.A., Welling, M., Muller, L.E.: Image segmentation with traveling waves in an exactly solvable recurrent neural network. Proceedings of the National Academy of Sciences **122**(1), 2321319121 (2025)

[17] Von Koeller, H.F., Schlemmer, A., Luther, S., Döring, Y., Voigt, N., Parlitz, U.: Analysing complex excitation patterns in cardiac tissue using wave event networks. Frontiers in Network Physiology **5**, 1674919 (2025)

[18] Pinto-Ramos, D., Martinez-Garcia, R.: How spatial patterns can lead to less resilient ecosystems. Proceedings of the National Academy of Sciences **123**(14), 2511994123 (2026)

[19] Jin, Q., Cui, D., Nelissen, K.: Dynamic spatiotemporal features in action recognition: a multimodal study. Communications Biology (2026)

[20] Xu, Y., Shen, X., Chen, R., Liang, W., Wang, P., Liu, J., Li, R.: Single-shot spatiotemporal characterization of ultrashort lasers based on spectral interferometry with fiber array. Communications Physics **9**(1), 151 (2026)

[21] Ribeiro, H.V., Zunino, L., Lenzi, E.K., Santoro, P.A., Mendes, R.S.: Complexity-entropy causality plane as a complexity measure for two-dimensional patterns. PLOS ONE (2012)

[22] Arizmendi, F., Barreiro, M., Masoller, C.: Identifying large-scale patterns of unpredictability and response to insolation in atmospheric data. Scientific Reports **7**(1), 45676 (2017)

[23] Sigaki, H.Y.D., De Souza, R.F., De Souza, R.T., Zola, R.S., Ribeiro, H.V.: Estimating physical properties from liquid crystal textures via machine learning and complexity-entropy methods. Physical Review E **99**(1), 013311 (2019)

[24] Tirabassi, G., Masoller, C.: Entropy-based early detection of critical transitions in spatial vegetation fields. Proceedings of the National Academy of Sciences **120**(1), 2215667120 (2023)

[25] Tirabassi, G., Duque-Gijon, M., Tiana-Alsina, J., Masoller, C.: Permutation entropy-based characterization of speckle patterns generated by semiconductor laser light. APL Photonics **8**(12) (2023)

[26] Tarozo, M.M., Pessa, A.A.B., Zunino, L., Rosso, O.A., Perc, M., Ribeiro, H.V.: Two-by-two ordinal patterns in art paintings. PNAS nexus **4**(3), 092 (2025)

[27] Gancio, J., Tirabassi, G., Masoller, C., Barreiro, M.: Detecting transitions and quantifying differences in two sst datasets using spatial permutation entropy. Earth System Dynamics **17**(3), 533–561 (2026)

[28] Kirkley, A.: Spatial regionalization based on optimal information compression. Communications Physics **5**(1), 249 (2022)

[29] Corso, G., Prado, T.d.L., Lima, G.Z.d.S., Kurths, J., Lopes, S.R.: Quantifying entropy using recurrence matrix microstates. Chaos: An Interdisciplinary Journal of Nonlinear Science **28**(8) (2018)

[30] Prado, T.L., Corso, G., Santos Lima, G.Z., Budzinski, R.C., Boaretto, B.R.R., Ferrari, F.A.S., Macau, E.E.N., Lopes, S.R.: Maximum entropy principle in recurrence plot analysis on stochastic and chaotic systems. Chaos: An Interdisciplinary Journal of Nonlinear Science **30**(4) (2020)

[31] Haralick, R.M., Shanmugam, K., Dinstein, I.: Textural features for image classification. IEEE Transactions on systems, man, and cybernetics (6), 610–621 (1973)

[32] Mallat, S.G.: A theory for multiresolution signal decomposition: the wavelet representation. IEEE transactions on pattern analysis and machine intelligence **11**(7), 674–693 (2002)

[33] Mandelbrot, B.B.: The fractal geometry of nature/revised and enlarged edition. New York (1983)

[34] Plotnick, R.E., Gardner, R.H., Hargrove, W.W., Prestegaard, K., Perlmutter, M.: Lacunarity analysis: a general technique for the analysis of spatial patterns. Physical Review E **53**(5), 5461 (1996)

[35] Maaten, L., Hinton, G.: Visualizing data using t-SNE. Journal of Machine Learning Research **9**(11) (2008)

[36] LeCun, Y., Bengio, Y., Hinton, G.: Deep learning. Nature **521**(7553), 436–444 (2015)

[37] Shannon, C.E.: A mathematical theory of communication. Bell System Technical Journal **27**, 379–423 (1948)

[38] Morel, C., Humeau-Heurtier, A.: Multiscale permutation entropy for two-dimensional patterns. Pattern Recognition Letters **150**, 139–146 (2021)

[39] Rostaghi, M., Humeau-Heurtier, A., Rostaghi, S., Azami, H.: Two-dimensional fuzzy dispersion entropy to nonlinear image analysis. Knowledge-Based Systems, 116144 (2026)

[40] Bandt, C., Pompe, B.: Permutation entropy: a natural complexity measure for time series. Physical Review Letters **88**, 174102 (2002)

[41] Eckmann, J.-P., Kamphorst, S.O., Ruelle, D.: Recurrence plots of dynamical systems. Europhysics Letters **4**(9), 973–977 (1987)

[42] Webber Jr, C.L., Zbilut, J.P.: Dynamical assessment of physiological systems and states using recurrence plot strategies. Journal of Applied Physiology **76**, 965–973 (1994)

[43] Marwan, N., Romano, M.C., Thiel, M., Kurths, J.: Recurrence plots for the analysis of complex systems. Physics Reports **438**(5-6), 237–329 (2007)

[44] Vasconcelos, D.B., Lopes, S.R., Viana, R.L., Kurths, J.: Spatial recurrence plots. Physical Review E **73**(5), 056207 (2006)

[45] Facchini, A., Mocenni, C., Vicino, A.: Generalized recurrence plots for the analysis of images from spatially distributed systems. Physica D: Nonlinear Phenomena **238**(2), 162–169 (2009)

[46] Facchini, A., Rossi, F., Mocenni, C.: Spatial recurrence strategies reveal different routes to turing pattern formation in chemical systems. Physics Letters A **373**(46), 4266–4272 (2009)

[47] Mocenni, C., Facchini, A., Vicino, A.: Identifying the dynamics of complex spatio-temporal systems by spatial recurrence properties. Proceedings of the National Academy of Sciences **107**(18), 8097–8102 (2010)

[48] Spezzatto, G.S., Flauzino, J.V.V., Corso, G., Boaretto, B.R.R., Macau, E.E.N., Prado, T.L., Lopes, S.R.: Recurrence microstates for machine learning classification. Chaos: An Interdisciplinary Journal of Nonlinear Science **34**(7) (2024)

[49] Bariviera, A.F., Hansen, R., Pastor, V.E.: Texture discrimination via hilbert curve path based information quantifiers. Pattern Analysis and Applications **28**(1), 1–18 (2025)

[50] Boots, B., Okabe, A., Sugihara, K.: Spatial tessellations. Geographical information systems **1**, 503–526 (1999)

[51] Krämer, K., Donner, R.V., Heitzig, J., Marwan, N.: Recurrence threshold selection for obtaining robust recurrence characteristics in different embedding dimensions. Chaos: An Interdisciplinary Journal of Nonlinear Science **28**(8) (2018)

[52] Boaretto, B.R.R., Andreani, A.C., Lopes, S.R., Prado, T.L., Macau, E.E.N.: The use of entropy of recurrence microstates and artificial intelligence to detect cardiac arrhythmia in ecg records. Applied Mathematics and Computation **475**, 128738 (2024)

[53] Mandelbrot, B.B., Van Ness, J.W.: Fractional brownian motions, fractional noises and applications. SIAM review **10**(4), 422–437 (1968)

[54] Barnsley, M.F., Devaney, R.L., Mandelbrot, B.B., Peitgen, H., Saupe, D., Voss, R.F.: The Science of Fractal Images. Springer, New York (1988)

[55] Turing, A.M.: The chemical basis of morphogenesis. Bulletin of mathematical biology **52**, 153–197 (1990)

[56] Barr, I.: Turing Patterns. Accessed: 2025-04-25 (2019). https://github.com/ijmbarr/turing-patterns/

[57] Kylberg, G.: The Kylberg Texture Dataset v. 1.0. External Report (Blue Series) No. 35, Centre for Image Analysis, Swedish University of Agricultural Sciences and Uppsala University. Available at https://user.it.uu.se/~gusky180/texture/ (2011)